Reconstruction of Aerial Images from Uniformly Sampled Magnitude Fourier Spectra using Spectral Statistical Models

Oliver M. Jeromin, *Student Member, IEEE*, and Marios S. Pattichis, *Senior Member, IEEE*

Abstract— **Statistical Kriging models for spatial data yield optimal linear estimates of unknown samples. In this work, we present a collection of statistical models defined over regions from a dyadic partition of the discrete Fourier spectrum. Spectral covariance models of the 2D Fast Fourier Transform (FFT) of aerial images allow for Kriging interpolation of magnitude and phase spectra from a small number of spectral samples. The reconstructed spectral components are compared to other widely used 2D interpolation algorithms (cubic splines, nearest neighbor, and bilinear interpolators). We approach this problem by exploring the magnitude and phase spectra independently.**

I. Introduction

SPECTRAL statistical covariance models, which we formally define in this work, calculated from transformed magnitude and phase spectral samples allow for the optimal linear estimates to be calculated of sparsely-sampled spectral data. Here, we apply this technique to remotely sensed satellite imagery.

This work is motivated by potential applications that include, but are not limited to, the development of better image compression schemas based on a limited number of spectral coefficients. In addition, other applications include the use of spectral interpolation methods for remote sensing modalities that directly sample the Fourier domain optically or electromagnetically, and also suffer from missing or degraded samples beyond and/or within the focal plane.

Formally, we reconstruct spectral data from uniformly spaced samples over a dyadic partition of the Fourier spectrum, utilizing separate models for the magnitude and phase, which allows for separate control of the reconstruction quality of each partition. A scalable solution that partitions the spectral domain into blocks of varying size allows for the use of appropriate covariance models of the magnitude and phase spectra bounded by the partitions ("spectral blocks") to be determined. The individual spectral models are then applied to solving for the optimal linear estimate, which is referred to in literature as Kriging [1].

The use of spectral data transformations are also presented as a means for producing data that is better suited for statistical modeling and variogram estimation. A logarithmic transformation is applied to the magnitude spectra, as it has been shown to impart intrinsic stationary over localized, bounded regions of the spectra. Phase spectra resulting from the 2D FFT can be best described as being uniformly randomly distributed over the interval of $-\pi$ to π. In this original state, the spectral samples fail to produce appropriate spectral statistical models that exhibit stationary inter-sample covariance. For phase spectra modeling, an unwrapping step is required to ensure that individual blocks can be effectively modeled using appropriate variogram models. The transformed magnitude and unwrapped phase spectra result in unique statistical models that are optimal over individual frequency blocks, which produce accurate spectral reconstructions that account for localized variability in the spectral domain.

Past papers that have been published on Kriging interpolation applications in remote sensing have all utilized a variation of spatial covariance models in which interpolation was applied to spatial image data [2-14]. The spectral covariance approach we present here has not yet been applied to digital image reconstruction in general and remote sensing imagery specifically.

The data sets used in this study were obtained from various multispectral image databases. Since satellite imagery varies widely based on the content in the scene being imaged, we intended to obtain a collection of images that could be described as depicting representative examples of rural, urban, and natural scenes. To compare performance across a wide variety of scene content, three rural images, five urban images, and two natural images were selected. The urban images are selected sub-regions of a single, large ASTER SpectroRadiometer sensor of London, England. Figure 1 depicts one sample image from each class.

(a) (b) (c)

Figure 1: Three images used in this study, sampled from the three image class types. (a) Purdue University Agronomy Research Center[1], size 1069x1374. (b) Sub scene from ASTER SpectroRadiometer image of London, England [2], size 401x501. (c) The Grand Canyon and surrounding country[3], size 351x501. Contact author for full list of image sources.

1.http://www.lars.purdue.edu/home/image_data/spectral_vision_data.html, Name: sv010813_ARC_F106_1m

2. http://photojournal.jpl.nasa.gov/catalog/PIA03402

3 http://asterweb.jpl.nasa.gov/gallery/images/london-final.jpg

O Jeromin is with the Department of Electrical and Computer Engineering at the University of New Mexico, Albuquerque NM, 87131, USA. Mr. Jeromin is the corresponding author. He can be reached by phone at: 505-284-8119 or by e-mail: ojeromin@ece.unm.edu.

M.S. Pattichis is with the Department of Electrical and Computer Engineering at the University of New Mexico, Albuquerque NM, 87131, USA (e-mail: pattichis@ece.unm.edu).

II. Theoretical Background

A. Spectral Statistical Models

The implication of discrete spectral interpolation goes beyond standard frequency domain image processing techniques such as image restoration. Various applications, such as magnetic resonance imaging (MRI), computed tomography (CAT scans), and synthetic aperture radar (SAR) sample data in the Fourier domain. Under certain conditions, such applications may be band-limited and the ability to interpolate Fourier data would provide improvement to the final data product (typically an image).

Here, we are interested in the discrete frequency spectrum lattice as indexed by (u_i, v_i). We shall denote the horizontal frequency coordinate with u_i and the vertical frequency coordinate with v_i. Borrowing from classical spatial statistics, we define the second-order stationary variogram as:

$$2\gamma(\mathbf{s}_1 - \mathbf{s}_2) = \mathrm{var}(Z(\mathbf{s}_1) - Z(\mathbf{s}_2)). \quad (1)$$

Assuming an intrinsically stationary random field, the method of moments estimator, commonly referred to as the classical variogram estimator, is given by:

$$2\hat{\gamma}(\mathbf{h}) \equiv \frac{1}{|N(\mathbf{h})|} \sum_{(i,j)\in N(\mathbf{h})} (Z(\mathbf{s}_i) - Z(\mathbf{s}_j))^2 \quad (2)$$

where $N(\mathbf{h})$ is defined by $N(\mathbf{h}) \equiv \{(i,j) : \mathbf{s}_i - \mathbf{s}_j = \mathbf{h}\}$ and $|N(\mathbf{h})|$ is the number of elements in the set $N(\mathbf{h})$. The classical estimator is **unbiased** but *not* **robust**.

Due to the periodic nature of the 2D FFT domain, intrinsic stationarity cannot be assumed over the entire spectrum. In order to have confidence in our variogram estimates, we sought a partitioned spectral domain that allowed independent spectral statistical modeling within the regions defined by the partition. We intentionally select a dyadic partition, which allows us to explore our spectral models using a scalable framework. The dyadic partitioning results in outer regions that are four times as large as the next smaller regions. These high frequency regions contain less spectral energy and we would like to perform more interpolation here. Conversely, the inner-most contain the low frequency information of the image and we want to preserve the original spectral content therein. Figure 2 depicts the half-spectrum partitions and numbers them for reference throughout this work.

For each spectral region, we sought to fit each magnitude and phase spectra empirical variogram with one of the following three theoretical semivariance models:

- The Spherical Model:

$$\gamma(\mathbf{h}) = \begin{cases} 0, & \mathbf{h} = 0, \\ \sigma + \alpha\{\frac{3}{2}(\|\mathbf{h}\|/\beta) - (\frac{1}{2}(\|\mathbf{h}\|/\beta)^3\}, & 0 < \|\mathbf{h}\| \le \beta, \\ \alpha + \sigma, & \|\mathbf{h}\| > \beta, \end{cases} \quad (5)$$
$$\sigma \ge 0, \alpha \ge 0, \text{and} \beta \ge 0.$$

- The Exponential Model:

$$\gamma(\mathbf{h}) = \begin{cases} 0, & \mathbf{h} = 0, \\ \sigma + \alpha\{1 - \exp(-\|\mathbf{h}\|/\beta)\}, & \mathbf{h} \ne 0, \end{cases} \quad (6)$$
$$\sigma \ge 0, \alpha \ge 0, \text{and} \beta \ge 0.$$

- The Gaussian Model:

$$\gamma(\mathbf{h}) = \begin{cases} 0, & \mathbf{h} = 0, \\ \sigma + \alpha\{1 - \exp - (\|\mathbf{h}\|^2/\beta^2) & \|\mathbf{h}\| \ne 0, \end{cases} \quad (7)$$
$$\sigma \ge 0, \alpha \ge 0, \text{and} \beta \ge 0.$$

In the above models, σ is the nugget effect, which was termed by Matheron as a representation of small scale variations (in our case, sub spectral sample variations) that manifest themselves as a discontinuity at the minimum measureable range value. α is referred to as the variogram sill, and it is defined as the limit of the variogram as the distance between samples approaches infinity. Typically, a good estimate for the variogram sill is the sample variance. Finally, β is referred to as the variogram range, and can be thought of as the lag at which $Z(\mathbf{s})$ and $Z(\mathbf{s}+\mathbf{h})$ are no longer correlated. It can be used a guide to determining the lag distances required to include in spatial prediction

B. Spectral Data Transformations

When a given spectral-domain region violates the above stationarity assumptions, it may be reasonable to expect that we can provide good, stationary, approximations over a disjoint partition of sub-regions of the original region. Furthermore, instead of requiring stationarity over the entire region, it is reasonable to assume that the **relative variogram,** defined by

$$2\gamma_Z^{(j)}(\mathbf{h})/\mu_j^2, \quad (4)$$

will remain approximately constant over all sub regions, independent of *j*. It can be shown that the application of the logarithmic transformation will produce an approximately intrinsically stationary random field over the entire region [1]. The importance of this result is that here, the logarithmic transformation allows us to apply our methods over the entire region within the dyadic partition, without requiring any knowledge of the specific boundaries of the constituent sub regions.

We applied various phase unwrapping techniques to the phase spectra, to provide better surfaces to model. Wrapped phase, being non-deterministic and distributed on the interval of $(-\pi, \pi]$ does not lend itself to covariance models. The 2-D phase unwrapping techniques are the three path following techniques: Goldstein's Branch Cut method, quality guided path following, and Flynn's minimum discontinuity method. The other two methods can be described as minimum norm methods, which approach phase unwrapping in a mathematically formal manner. These are the preconditioned

conjugate gradient (PCG) algorithm and the weighted multigrid algorithm [15].

C. Optimal Interpolation Using Kriging

Assuming that each spectral location can be modeled by the constant mean and random noise model, $Z(\mathbf{s}) = \mu + n(\mathbf{s}), \quad \mathbf{s} \in F, \quad \mu \in \Re$, ordinary Kriging, estimates the optimal linear predictor using a weighted sum of the known data points within a region, **B**:

$$p(\mathbf{Z};\mathbf{B}) = \sum_{i=1}^{n} \lambda_i Z(\mathbf{s}_i) \cdot \tag{9}$$

Since we assume that the random field model is zero-mean, we also require that the optimal data points should satisfy:

$$\sum_{i=1}^{n} \lambda_i = 1, \tag{10}$$

which guarantees uniform unbiasedness.

Numerical optimization techniques are used to minimize the prediction error with respect to the selected spectral statistical model values ($\lambda_1, \lambda_2, \ldots, \lambda_n$) and the resulting Lagrange multiplier that ensures the constraint holds resulting in a system of linear equations. The computational complexity of the Kriging interpolation step is dependent on the size of the linear system. In matrix form, the solutions computational complexity is governed by a matrix inversion of size $N \times N$, where N is the number of interpolated samples being sought.

III. METHODS

Using a dyadic partition of the Fourier Spectrum, we can apply sampling rates to each of the partitions shown in Figure 2. The independent control of various spectral regions allows for independent control of high, medium, and low frequency reconstructions. We explored the effective sampling rates in Table I.

A. Variogram Model Selection and Fitting

We considered three variables when selecting the appropriate model for the empirical variograms calculated within each spectral partition. First, we assume that the isotropy holds, which implies that the variogram model is unidirectional (a function of lag alone). Non-isotropic models require additional computational complexity and reduce the number of discrete spectral values in the variogram estimator. An anisotropic model that considers N discrete directions to fit the continuum of possible directions will utilize only $\sim 1/N$ of the total samples that would be available to the isotropic model. Because the portions of the spectrum represented by the frequency blocks in which we sample are continuous, we can define our models with fewer samples in the discrete frequency plane. It is important to realize that the number of samples is not indicative of distance. Even though the 2D FFT generates uniform FFT samples, other discrete signal processing methods can generate an arbitrary number of samples in any of the continuous, bounded spectral blocks. One way to accomplish this would be by using the Chirp-Z transform, which generates any number of samples in any continuous bounded region within the Fourier domain [16].

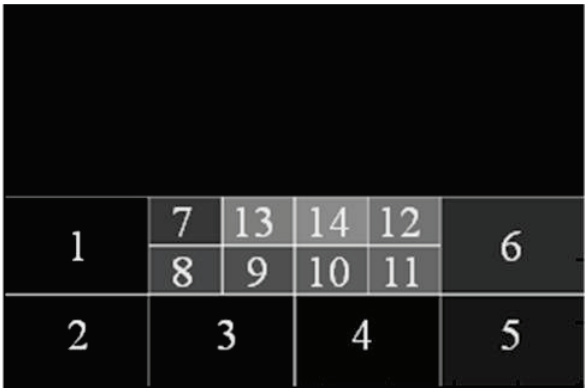

Figure 2: Spectral partition map. The partitions shown above define the regions of the spectral data which we model individually for analysis. The original size of the image used to generate this map was 301x401 pixels. The spectral data contained in regions 13 and 14 was not included in any of the down sampling rates used in this study. The sizes of the outer regions for this mask are 75x112 pixels, while the sizes of the inner regions are 37x56 pixels.

The second consideration required when calculating variogram models is the extent of the range that will be used in the variogram estimation. The additional computational cost of variogram calculation over the entire frequency block was chosen as part of the variogram estimation process. This ensures that our method is scalable; allowing multiple sampling rates within a single frequency partition to be explored based a single estimate of the variogram. In other words, we ensure that the estimated model provides a semivariance for the largest possible sampling rate.

Finally, the third consideration that is required is how many semivariance values to fit and which model best fits the empirical data. We appeal to numerical optimization to determine which model via non-linear least squares curve fitting. The sampling rate applied to each spectral partition will be used to govern the size of the maximum lag we wish to fit the model to.

B. Kriging Interpolation of Magnitude and Phase Spectra

Simple Kriging is used based on the magnitude and phase variogram estimates, providing the optimal linear estimator of the missing FFT samples. Two parameters were explored in finding the optimal Kriging result: the *max-distance* and the *max-samples* values. Here, the *max-distance* parameter refers to the circular radius of the maximum discrete-frequency space distance that needs to be considered for estimating the

TABLE I
SPECTRAL STATISTICAL DATA SAMPLE RATES

MAGNITUDE / PHASE	4x/16x	16x/64x	64x/256x
NONE: 1x/1x	18.75%	11.97%	10.17%
1x/4x	17.26%	15.57%	15.12%
4x/16x	9.38%	7.68%	7.23%
16x/64x	7.68%	5.99%	5.54%

missing value. For Kriging, all known FFT sample values that fall within the circle with radius max-distance are used for estimating the missing value. The max-samples refers to the exact maximum number of known FFT samples that need to be considered for providing the optimal estimate. The idea is that the number of available samples is a function of the location of the unknown missing value. We chose to explore values of *the* max-samples parameter, as it is not prone to geometric constraints along the edges of the frequency blocks and provides consistent reconstruction models.

Using the max-samples value that provides the best reconstruction (in terms of peak signal-to-noise ratio or PSNR), we reconstructed both the magnitude and the unwrapped phase spectra of each of the two-dimensional phase unwrapping techniques. We compared both the reconstructed magnitude samples from the Kriging method here to other two-dimensional interpolation algorithms: the nearest-neighbor, bilinear, and spline interpolators [17] using the PSNR. The Kriging results of the various phase unwrapping techniques are compared to discern which unwrapping method best suits this application. We leave further comparison of the reconstructed images to other two-dimensional interpolation techniques for the future.

IV. RESULTS

A. Variogram Range Selection, Estimation, and Fitting

We present the estimated variograms based on spectral block classification (high or medium), spectra type (magnitude and phase), and image type (rural, urban, or natural). variogram was fitted using the distance associated with a reduction of the FFT sampling rate by 8 in each dimension for the high frequency blocks and by 4 in each dimension for the middle frequency blocks. Thus, one out of every 64 samples in the high frequency blocks was kept and one out of every 16 samples in the medium frequency blocks. The calculated parameters from the fit are tabulated for the natural image shown in Figure 1(c) are presented in Table II and reveal that our methods do result in tractable estimates that are represented by meaningful model parameter values.

We also include the spectral data images and fitted variograms for two entries in Figure 2 – the log-transformed magnitude variogram from spectral block 8 and the Flynn's Minimum Discontinuity unwrapped phase variogram from spectral block 2.

Block #8, Log-Transformed Magnitude

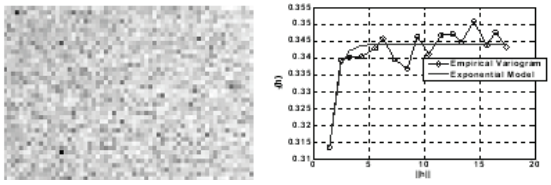

Block #2, Log-Flynn's Unwrapped Phase

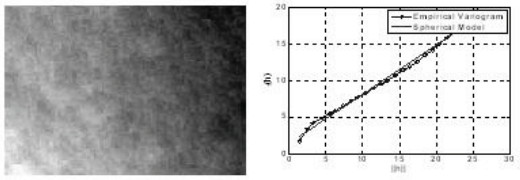

Fig. 2. Examples of fitted magnitude and unwrapped phase variogram estimates and fitted models. The top (magnitude) surface was fit with an Exponential model using $\sigma = 0.1930$, $\alpha. = 0.1535$, and $\beta = 0.9115$. The bottom (phase) surface was fit with an Spherical model with $\sigma = 1.4454$, $\alpha. = 3.1683\text{e-}3$, and $\beta = 7.086\text{e-}3$.

From the variogram plots in Figure 2 we note that the number of variogram coefficients that were fit for the high frequency blocks was truncated to be 25, since the high frequency sample rate was one out of every eight samples. The radial lag spanning three samples in each dimension is 33.94, which is beyond the limit we have found to produce the best fits. The medium frequency blocks are fit out to a lag of 17, since the sample rate in these blocks is one out of every four samples. These plots are a good representation of the adaptive and scalable solution our method provides

B. Magnitude and Phase Kriging.

Table II contains non-parametric summary statistics of the high frequency block *magnitude* reconstruction PSNR values over all ten images. We included the best performing comparison method: the linear interpolator. The above results were obtained by fitting the minimum number of semivariance values up to either a radius of 25 for sample rates greater than 8; or the radial distance equal to three times the sampling rate for sample rates less than 8. The Kriging steps were performed using the derived max-samples from a max-distance parameter value of 25 for the high frequency blocks and 20 for the medium frequency blocks. Experiments

TABLE II
HIGH FREQUENCY BLOCK RECONSTRUCTION PSNR, MAGNITUDE

	Statistic / Sampling Rate	Min	1st Quartile	Median	3rd Quartile	Max
KRIGING	16x	**44.9250**	**50.2470**	**52.1638**	**53.3509**	**55.0397**
	8x	**46.7038**	**51.6753**	**53.7825**	**54.7097**	**56.7870**
	4x	**46.7038**	**53.4854**	**55.1832**	**55.7543**	**57.7496**
BILINEAR	16x	45.7441	49.1677	51.5058	52.3860	53.7980
	8x	46.7093	50.2485	51.4099	52.5443	54.2441
	4x	47.2029	51.2519	52.2092	52.9615	54.7953

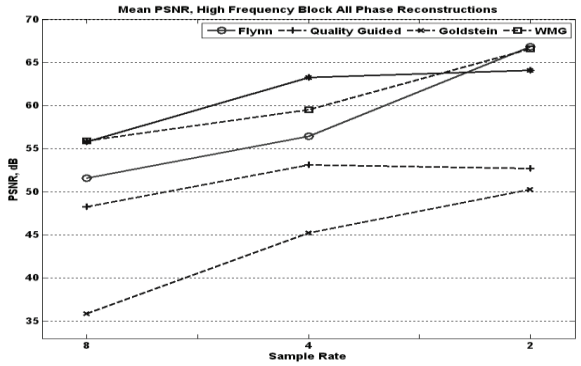

Figure 3: High frequency block unwrapped phase reconstruction using Kriging to compare unwrapping methods. The mean PSNR of the high frequency block reconstructions are shown.

on both the high and medium frequency blocks revealed that these are the optimal parameter values. Going beyond 25 neighbors does not gain significant improvement in reconstructions. The additional computational cost is not worth an unperceivable gain in reconstruction quality.

Figure 3 contains the PSNR values of the high frequency reconstructed unwrapped phase surfaces. The best method, quantitatively, is the preconditioned gradient technique, followed by WMG and Flynn's method. Due to the significantly number of less unwraps performed by Flynn's method, which will result in a lower relative error value, we feel this method is best suited for the Kriging techniques for phase spectra estimation. In addition, Flynn's method doe not require as much optimization, which may be a considerable result in computational costs.

V. Conclusion

In this paper, we have developed a spectral covariance modeling technique and Fourier spectra reconstruction method by extending geostatistical theory to the discrete Fourier domain. We found that the problem of spectral modeling is well suited for scalability, in which magnitude and phase sampling is performed in a manner that the frequency content with more energy (which, for naturally occurring images, is located at the center of the spectrum) is given greater importance in governing the spatial image quality. Therefore, we proposed combinations of sampling rates that are applied separately to the high and medium frequency blocks generated by the dyadic partitioning of the spectral surfaces.

The large number of Kriged phase blocks allowed for a quantitative comparison between phase unwrapping methods. The path following phase unwrapping algorithms result in unique phase surfaces. We have shown that some unwrapping methods result in phase surfaces that are better suited for our spectral statistical modeling approach. It was shown that both the Flynn's Minimal Discontinuity and both minimum norm methods (Weighted Multi-Grid and Preconditioned Conjugate Gradient) resulted in much better block reconstructions. Our decision to implement Flynn's method was due to the fact that it generally results in a smaller range in the unwrapped values, from which localized interpolation values will result in a smaller absoluter error when the inverse 2D FFT is applied to the reconstructed magnitude and phase spectra.

This paper summarizes the techniques employed to explore the parameter space of our spectral estimation method using statistical models and ordinary Kriging. Future work will focus on quality assessment of the synthesized images resulting from the interpolated magnitude and phase spectral components and compare the results using the method presented here to other spectral data compression schemes.

Acknowledgement

The research presented in this paper has been funded by the Air Force Research lab under grant AFRL Award #FA9453-09-C-0309.

References

[1] N. A. Cressie. *Statistics for Spatial Data*. John Wiley and Sons, New York, revised edition, 1993.

[2] K. Cheng, H.Yeh, and C. Tsai, "An anisotropic modeling approach for remote sensing image rectification," *Remote sensing and the environment*, vol. 73, pp. 46-54, 2000.

[3] P. S. Kanarolgou, N. A. Soulakellis, and N. I. Sifakis, "Improvement of satellite derived pollution maps with the use of a geostatistical interpolation method," Journal *of Geographic Systems,* vol. 4, pp. 193:208, 2002.

[4] R. E. Rossi, J. L. Dungan, and L. R. Beck, "Kriging in the shadows: geostatistical interpolation for remote sensing," *Remote sensing and the environment,* vol. 49, pp. 32-40, 1994.

[5] A. Ferretti, C. Prati, and F. Rocca, "Permanent scatterers in SAR interferometry," *IEEE Trans. On Geoscience and Remote Sensing,* vol. 39, pp. 8-20, 2001.

[6] T. Blaschke, "Object-based contextual image classification build on image segmentation," In *IEEE workshop on advances in techniques for analysis of remotely sensed data*, pp. 113-119, October, 2004.

[7] J. Djamdji and A. Bijaoui., "Disparity analysis: a wavelet transform approach," *IEEE Trans. On Geoscience and Remote Sensing*, vol. 33, pp. 67-76.

[8] T. Pham and M. Wagner, "Image restoration by fuzzy convex ordinary kriging," In *Proceedings of the international conference on image processing*, vol. 1, pp. 113-116, September 2000.

[9] W. Oh and B. Lindquist, "Image thresholding by indicator kriging," *IEEE Trans. on Pattern Analysis and Machine Intelligence*, vol. 21, pp. 590-602, 1999.

[10] S. Chandra, M. Petron, and R. Piroddi, "Texture interpolation by ordinary kriging," In *Pattern recognition and image analysis,* vol. 3523, pp. 183-190, 2005.

[11] J. R. Carr, "Spectral and textural classification of single and multiple band digital images," *Computer and Geosciences*, vol. 22, pp. 1063-1079, 1990.

[12] E. Decenciere, C. Fouquet, and F. Meyer, "Applications of kriging to image sequence coding," *Signal processing: image communication*, vol. 13, pp 227-249, 1998.

[13] B. Grinstead, A. Koschan, and M. A. Abidi, "Geometry refinement of 3D surfaces using kriging," In *Proceedings of the Third International Symposium on 3D Data Processing, Visualization, and Transmission (3DPVT'06)*, pp. 719-726, 2006.

[14] A. Panagiotopoulou and V. Anastassopoulos, "Super-resolution image reconstruction employing kriging interpolation technique," *14th International Workshop on Systems, Signals, and Image Processing*, pp. 144-147, June 2007.

[15] D. C. Ghiglia and M. D. Pritt, Two-Dimensional Phase Unwrapping: Theory, Algorithms, and Software, John Wiley and Sons, New York, 1998.

[16] L. Rabiner, "The chirp z-transform algorithm – A lesson in serendipity, IEEE Signal Processing Magazine, March 2004, pp. 118-119.

[17] C. de Boor, A practical guide to splines, revised edition, Springer-Verlag, New York, 2001.